International Journal of Impact Engineering 37 (2010) 250–259

Contents lists available at ScienceDirect

International Journal of Impact Engineering

journal homepage: www.elsevier.com/locate/ijimpeng

Split Hopkinson pressure bar multiple reloading and modeling of a 316 L stainless steel metallic hollow sphere structure

A. Taşdemirci, Ç. Ergönenç, M. Güden*

Dynamic Testing and Modelling Laboratory and Department of Mechanical Engineering, Izmir Institute of Technology, Gulbahce Koyu, Urla, Izmir, Turkey

ARTICLE INFO

Article history:
Received 5 February 2009
Received in revised form
21 May 2009
Accepted 21 June 2009
Available online 27 June 2009

Keywords:
Metallic hollow sphere
Split Hopkinson bar
High strain rate
LS-DYNA
Multiple loading

ABSTRACT

The high strain rate (600 s^{-1}) compression deformation of a 316 L metallic hollow sphere (MHS) structure (density: 500 kg m^{-3}; average outer hollow sphere diameter: 2 mm and wall thickness: 45 μm) was determined both numerically and experimentally. The experimental compressive stress–strain behavior at high strain rates until about large strains was obtained with multiple reloading tests using a large-diameter compression type aluminum Split Hopkinson Pressure Bar (SHPB) test apparatus. The multiple reloading of MHS samples in SHPB was analyzed with a 3D finite element model using the commercial explicit finite element code LS-DYNA. The tested MHS samples showed increased crushing stress values, when the strain rate increased from quasi-static (0.8×10^{-4} s^{-1}) to high strain rate (600 s^{-1}). Experimentally and numerically deformed sections of MHS samples tested showed very similar crushing characteristics; plastic hinge formation, the indentation of the spheres at the contact regions and sphere wall buckling at intermediate strains. The extent of micro-inertial effects was further predicted with the strain rate insensitive cell wall material model and with the strain rate sensitive behavior of MHS structure similar to that of the cell wall material. Based on the predictions, the strain rate sensitivity of the studied 316 L MHS sample was attributed to the strain rate sensitivity of the cell wall material and the micro-inertia.

1. Introduction

Metal foams are known to be light-weight structures, which absorb relatively high amount of deformation energies under dynamic loading conditions. Since, the energy absorption occurs nearly at a constant stress until about large crushing strains, metal foams have the capabilities of impact energy absorption at very high efficiencies. However, the processing routes of metal foams result in unavoidable variations in cell size, cell wall thickness and the formation of imperfections including curved and missing cell walls and nodes on the cell edges. These lead to high reductions in load carrying capacities [1] and large variability in measured mechanical properties [2]. Metallic hollow sphere (MHS) structures are however characterized with their regular cellular structures; hence, show relatively small variations in stress–strain behavior. This potentially makes MHS structures suitable for the applications in which the metal foams are used, including light-weight filler for the columnar structures and core materials in sandwich panels.

The experimental quasi-static compression mechanical behavior of MHS structures were previously investigated [3–5]. Few studies were also on the dynamical behavior [6,7] and on the modeling of the mechanical properties [8–10]. Previous numerical models performed to predict the mechanical behavior of MHS structures were mostly based on the unit cell approximation which accounted merely the individual hollow sphere deformation [6,8–10]. To the authors' knowledge, there has not been any study on the numerical modeling of whole MHS structure in Split Hopkinson Pressure Bar (SHPB) high strain rate testing. The testing of metallic cellular structures in a conventional SHPB set-up for the determination of the high strain rate mechanical response at increasing strain values is also problematic in a single shot test due to the lower final strains attained. To increase the final strain values in a single SHPB test, very long bars and small thickness of the test sample and diameter should be used. Alternatively, the stress values of cellular materials at relatively large strains can be obtained by applying reloading test in a single SHPB testing. In this study, a 316 L stainless steel MHS structure was tested through SHPB multiple reloading experiments to reach relatively large strains. The multiple loading was modeled on

* Corresponding author. Mechanical Engineering Department, İzmir Institute of Technology, Gulbace koyu, 35430 Urla, Izmir, Turkey. Tel.: +90 232 7507816; fax: +90 232 7507890.
E-mail address: mustafaguden@iyte.edu.tr (M. Güden).

0734-743X/$ – see front matter © 2009 Elsevier Ltd. All rights reserved.
doi:10.1016/j.ijimpeng.2009.06.010

a MHS specimen comprising the similar number of hollow spheres as with experiments. The model assumed perfect cubic packing of the spheres and allowed to analyze the effect of strain rate sensitivity of the cell wall material and micro-inertia on the high strain rate deformation of MHS structures.

2. Materials and testing

As-received sintered 316 L stainless steel metallic hollow sphere (MHS) cylindrical compression test specimens were produced by Fraunhofer Resource Center. Test specimens, 20 mm in diameter and 20 mm in height (Fig. 1(a) and (b)), were cut into the final geometry using an electrical discharge machine by the producer. The processing details of the random MHS structures are given in ref. [3]. The processing route simply consists of coating of Styrofoam spheres (used as core) with 316 L powder in a fluidized bed using a binder solution, shaping the green spheres in a die and finally sintering the shaped green hollow spheres at a high temperature. The density of as-received MHS specimens was 500 kg m^{-3}, corresponding to a relative density of 7.24% (density of stainless steel was taken 6900 kg m^{-3} [3]). The shaping of the green spheres to form MHS structure unavoidably resulted in the formation of flat contact regions between the spheres as depicted in Fig. 2. The geometrical parameters for the studied MHS structure shown in Fig. 2 are the outer diameter (D) and the thickness (t) of the spheres and the bonding angle (θ) between spheres. These parameters for the studied MHS structure were determined through the measurements (at least 20 measurements) performed on the scanning electron microscope (SEM) pictures. The average outer diameter and the thickness of the spheres and the bonding angle were found 2 mm, 45 μm and 20°, respectively.

Quasi-static compression tests were conducted using a displacement controlled Shimadzu AG-I universal tension-compression test machine at a cross-head speed of 0.1 mm min^{-1} corresponding to a nominal strain rate of $\sim 0.8 \times 10^{-4}$ s^{-1}. High strain rate tests (550–650 s^{-1}) were performed using a compression type SHPB. The used SHPB apparatus comprises three 40.05 mm diameter-aluminum bars (7075-T6 Al): a striker bar 600 mm in length, an incident bar and a transmitter bar 1550 mm in length. The modulus and density of the bar material are 70 GPa and 2700 kg m^{-3}, respectively. With the use of equal length incident and transmitter bars, the same specimen was deformed repeatedly in a single SHPB test. The loading of the specimens

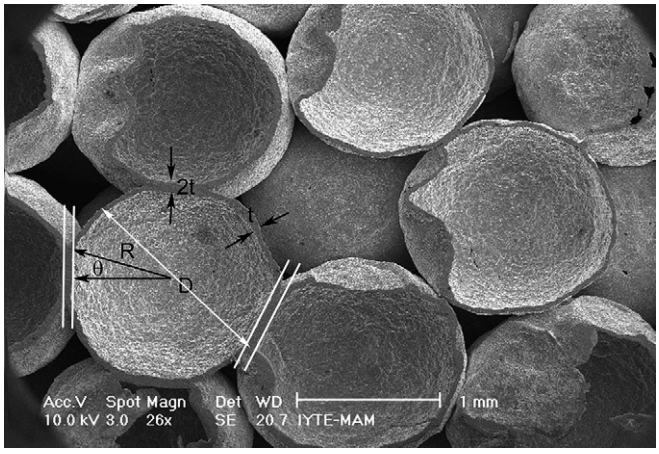

Fig. 2. SEM picture of hollow spheres and the geometrical parameters.

during SHPB tests was captured at a frame rate of 5000 fps using a Fast-Cam high speed video camera. The specimens deformed until about a certain strain for the microscopic studies were recovered by placing large diameter ring-shaped steel collars of different lengths to restrict the axial strain in the specimen, similar to the method used in [11]. The collars were loose-fitted and imposed no radial constraint to MHS samples.

The strain rate ($\dot{\varepsilon}$), strain (ε) and stress (σ) in the specimen in SHPB testing are calculated using the following equations based on one-dimensional wave propagation in long bars:

$$\dot{\varepsilon}(t) = \frac{-2C_b}{L_s}\varepsilon_r(t) \tag{1}$$

$$\varepsilon(t) = \frac{-2C_b}{L_s}\int_0^t \varepsilon_r(t)\mathrm{d}t \tag{2}$$

$$\sigma(t) = \frac{E_b A_b}{A_s}\varepsilon_t(t) \tag{3}$$

where, C_b is the elastic wave velocity of the bar, L_s is the sample length, E_b is the modulus of the bar material and A_s and A_b are the

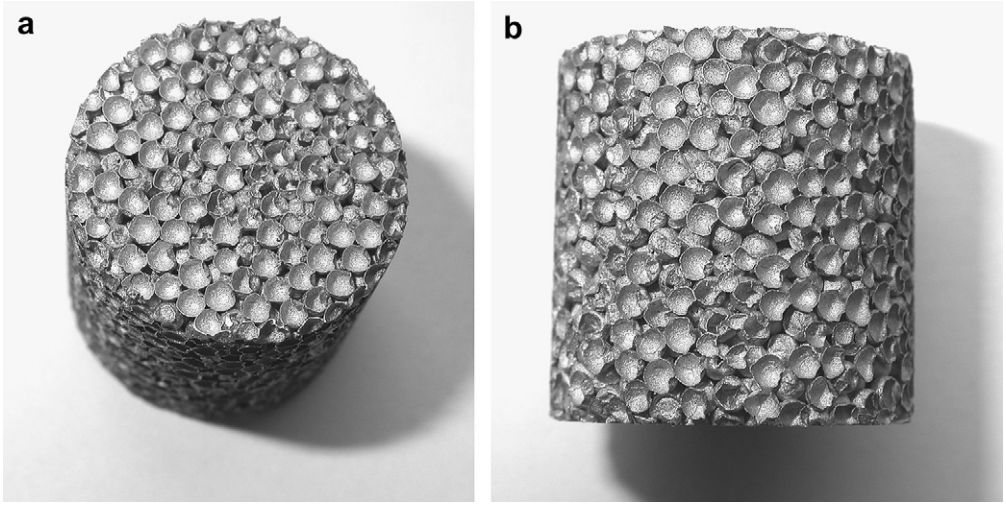

Fig. 1. Cylindrical MHS test sample; (a) top and (b) side view.

sample and bar cross-sectional areas respectively. ε_r and ε_t are the reflected and transmitted strains measured from strain gages on the bar, respectively. At least three compression tests were performed at quasi-static and high strain rate tests.

3. Modeling

A 3D finite element model of SHPB was used to investigate the dynamic deformation behavior and the stress state of the MHS structures (Fig. 3(a) and (b)). The analyses were performed using the commercial explicit finite element code LS-DYNA 971 [12]. For each test modeled, the force and, hence, the stress values were calculated at several locations within the sample, including the sample front and back surfaces, as well as at the location of the strain gages on the incident and transmitter bars of the SHPB apparatus. The model has four components in contact; a striker bar of length 600 mm, an incident bar and a transmission bar each of length 1550 mm and the specimen of length and diameter of 20 mm. An initial velocity of 12.5 m s^{-1}, the same as SHPB experiments, was assigned to the striker bar. Since two axes of symmetry were assumed in the model, only one-quarter of the bar was modeled (Fig. 3(b)). The components of SHPB set-up were modeled with eight-node solid elements.

A total of 75 elements were used in the model for the cross-section, which provided 10 elements across the radius of the bars and a total of 400 elements were used along the length of the bar. Mesh biasing along the bar axis was applied to refine the meshes at the contact interfaces. Initially, the simple cubic unit cell of the MHS structure was meshed with 480, 640 and 1120 shell elements and placed between moving top and fixed bottom rigid walls. The unit cell was loaded with a velocity controlled rigid wall and the load-displacement curves have shown that 640 shell elements was able to give converged solutions within a reasonable amount of time. The numerical model therefore included 162,642 shell elements (640 elements for each sphere) for the specimen and 65,550 solid elements for the striker, incident and transmitter bars. The MHS

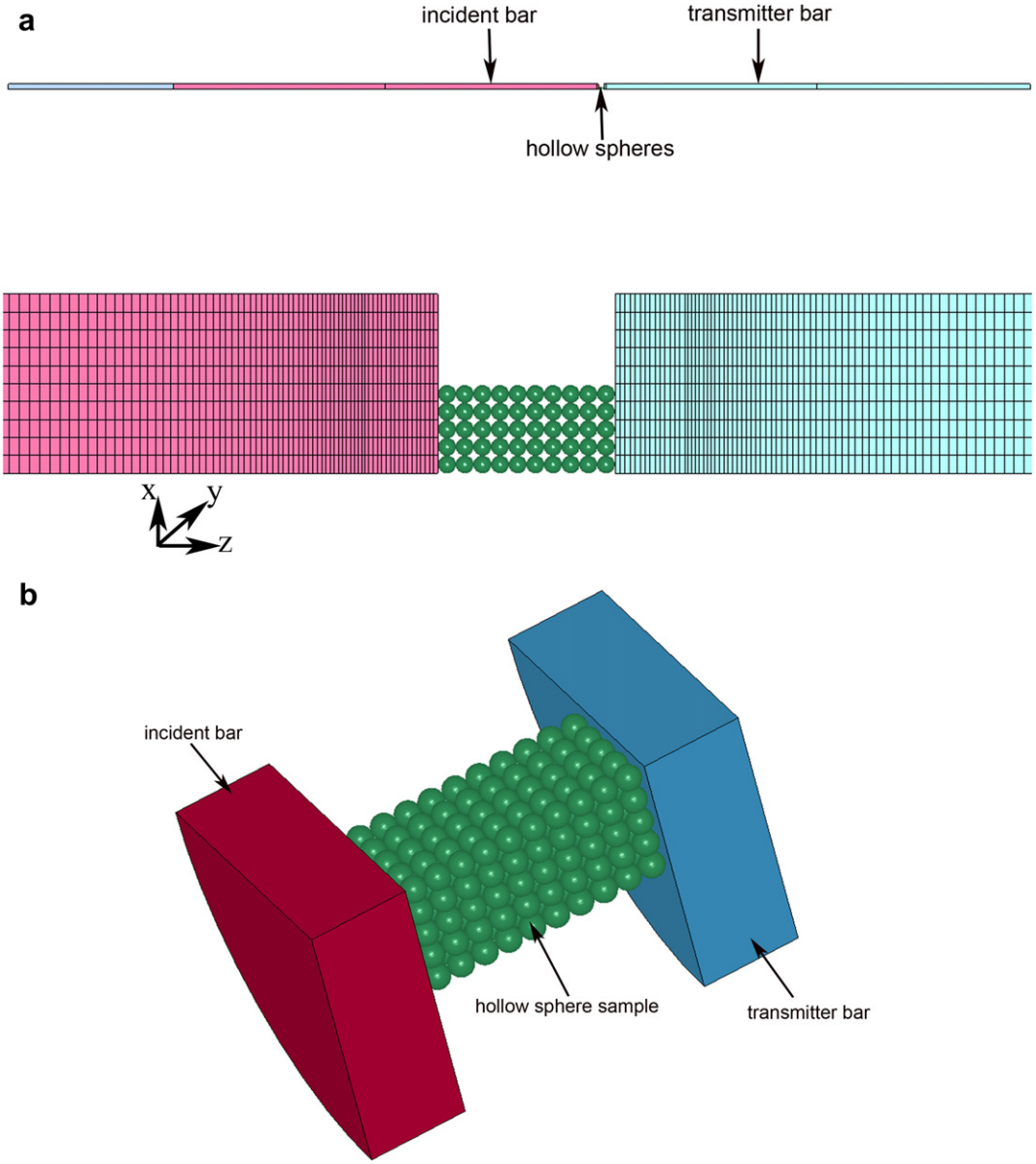

Fig. 3. SHPB test numerical model: (a) model with bars and (b) MHS model between the bars.

structure was modeled using Belytschko–Tsay shell element with five integration points through the thickness. For time step calculation, the automatic time step calculation option was chosen. In this option LS-DYNA determines the initial time step size. During the solution, LS-DYNA loops through the elements and determines a new step size by taking the minimum value over all elements. Individual spheres were assumed as perfectly bonded (tied) at the flat contact surfaces. Symmetry boundary conditions were employed in the numerical model of MHS structure. For x–z plane, the translation of the nodes along y direction and the rotations of the nodes along x and z directions were not allowed (Fig. 3). For x–y plane, the translation of the nodes along x direction and the rotations of the nodes along y and z directions were not allowed. In addition, there were two symmetry planes defined on x–z and y–z planes in order to prevent the non-physical motion of the inner nodes that were not on the planes but close during the course of the deformation. For the MHS structure, including the spheres and the contacting faces of the bars, an automatic single surface contact was adopted to account for the contact between the individual spheres and the contact between whole sphere structure and the bar surfaces. Individual spheres were assumed as perfectly bonded at the flat contact surfaces.

Force equilibrium in the specimen was further checked numerically using a dimensionless number, R, given as [13],

$$R = \frac{2(F_1 - F_2)}{(F_1 + F_2)} \tag{4}$$

where, F_1 and F_2 are the forces between specimen-incident and specimen-transmitter bar interfaces, respectively. Further details of the SHPB modeling procedure is found elsewhere [14].

The relative density of sintered MHS structure without bonding agent between spheres is given as [10],

$$\frac{\rho^*}{\rho} = PF \times \left[3\left(\frac{t}{R}\right) - 3\left(\frac{t}{R}\right)^2 + \left(\frac{t}{R}\right)^3\right] \tag{5}$$

where, ρ^* and ρ are the density of MHS sample and the wall material, respectively, PF is the sphere packing factor; being 0.52, 0.68 and 0.74 for the simple, body-centered and face-centered cubic packing, respectively, and R is the outer radius of the hollow sphere. Using the typical values for the studied MHS sample ($\rho = 500\ \mathrm{kg\,m^{-3}}$, $t = 45\ \mu\mathrm{m}$ and $R = 1\ \mathrm{mm}$) in Eq. (5), the density of MHS are calculated 463, 605 and 659 $\mathrm{kg\,m^{-3}}$ for simple, body-centered and face-centered cubic packing geometries, respectively.

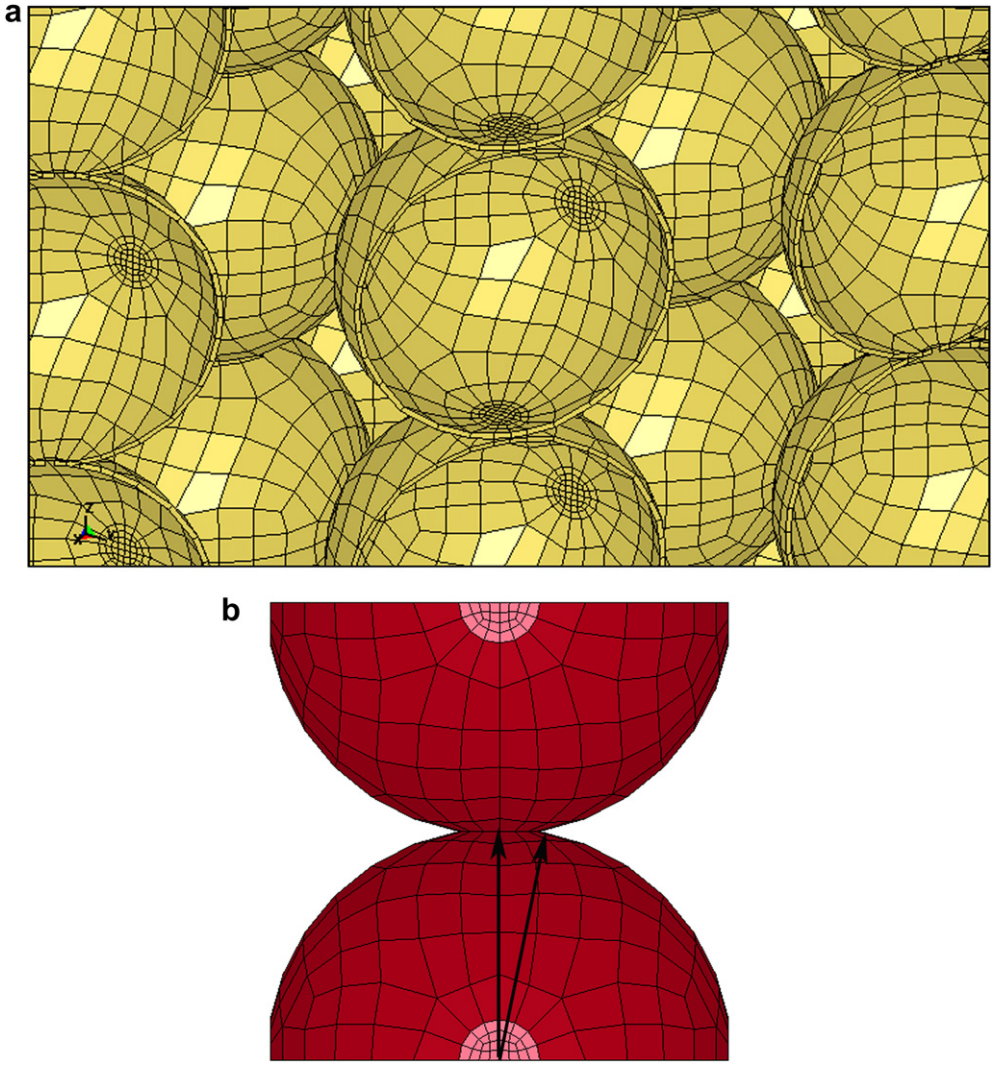

Fig. 4. (a) The cubic packing of hollow spheres, showing the contact points and (b) a flat contact region between two spheres.

Table 1
Material properties used in finite element model.

Material	Modulus of Elasticity (GPa)	Poisson's ratio	Density (kg m^{-3})	Yield stress (MPa)	C (s^{-1})	p
Aluminum	70	0.3	2700	–	–	
316 L	115	0.3	6950	255	429	4.08

Since the density of the studied MHS structure (500 kg m^{-3}) was found similar to the density of the simple cubic packing, a simple cubic packing of spheres was assumed in the model. Simple cubic packing structure has a coordination number of 6; hence, each hollow sphere has 6-contact points with adjacent spheres. Fig. 4(a) and (b) show the contact points between the spheres in the model and a contact region between two spheres, respectively. A finer meshing is adapted to the contact points of the spheres as depicted in Fig. 4(a). The bonding between the spheres is also assumed to be flat with a bonding angle of 20° (Fig. 4(b)), the same with the MHS structure tested.

The aluminum bars of SHPB were modeled with an isotropic elastic material model. The cell wall material of MHS structure was modeled with *MAT_PLASTIC_KINEMATIC (material 3) material model. In this model, the constitutive behavior of the 316 L stainless steel was described with a linear-elastic/perfectly-plastic material model with von Mises yield criteria. The strain rate sensitivity of 316 L stainless steel was accounted by adding Cowper–Symonds term to the constitutive relation as,

$$\frac{\sigma^*}{\sigma} = 1 + \left(\frac{\dot{\varepsilon}}{C}\right)^{\frac{1}{p}} \tag{6}$$

where, σ^* is the stress at a strain rate of $\dot{\varepsilon}$, σ is the stress at the reference strain rate and C and p are the material constants. The material model parameters of aluminum bars and the cell wall material used in the modeling of MHS structure are tabulated in Table 1. The strain rate parameters of 316 L stainless steel, C and p were taken as 429 s^{-1} and 4.08 [15], respectively, and the other material model parameters were taken from ref [6].

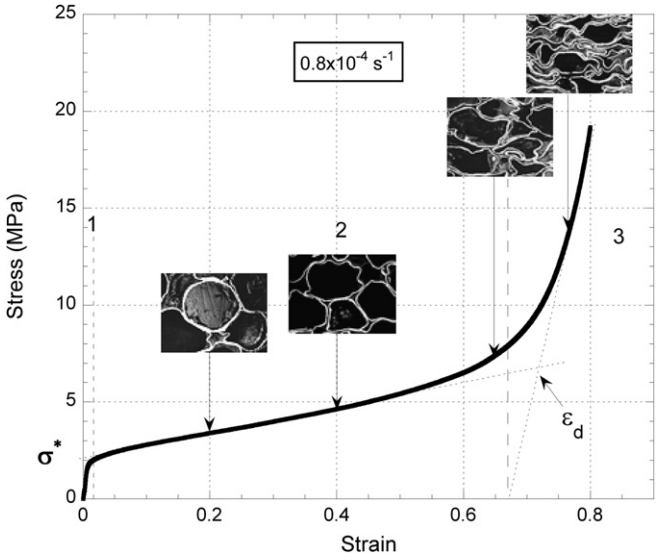

Fig. 5. Typical quasi-static stress–strain curves of MHS samples.

4. Results

Fig. 5 shows typical engineering stress–strain curve of MHS samples tested quasi-statically. As with other cellular structures such as aluminum closed-cell foams, MHS structures show characteristic compressive stress–strain curves, comprising three distinct deformation regions: linear elastic, collapse and densification regions as marked with 1, 2 and 3 in Fig. 5. In the inset of Fig. 5, the deformed sections of a tested MHS sample are shown at various strain levels. Fig. 6(a) and (b) further show high strain rate experimental and numerical deformed sections of MHS samples at various strains, respectively. In the linear elastic region, the deformation is presumably controlled by the sphere wall bending and/or stretching. The elastic region is followed by a collapse region occurring as noted previously [16] by the plastic hinge formation and the indentation of the spheres at the contact regions (collapse region) (Fig. 7(a)). In addition to sphere indentation, the sphere cell wall buckling in between adjacent spheres at the intermediate strain levels (Fig. 7(b)) is observed in the collapse region. The collapse region is generally characterized by a *collapse stress* (σ^*). The collapse stress (2.12 MPa) was determined as the intersection of the stress axis to a linear line fitted to the collapse region, similar to the method used in [3]. The sphere deformation proceeds until about the flattening of the spheres in a direction normal to the compression loading axis at relatively large strains. The densification strain, ε_d, (0.71) is taken as the intersection of the tangents to the stress plateau regime and densification regime [17,18] as shown in Fig. 5. In the densification region the flattened cell walls are compressed all together (Fig. 7(c)), resulting in a sharp increase in the stress values (region 3 of Fig. 5). The deformation mechanisms explained above was determined to be the same for both quasi-statically and dynamically tested specimens, showing a very much similar deformation mechanisms for the MHS specimens tested within the studied strain rate regime.

Fig. 8(a) and (b) show the experimental and numerical incident, reflected and transmitted stresses as function of time in a multiple loaded MHS specimen in SHPB. The MHS specimen is repeatedly loaded with compressive waves returning from the free end of the incident bar as shown by the consecutive numbers in Fig. 8(a) and (b). The stress values shown in Fig. 8(a) and (b) are very similar, showing the capabilities of the used model to predict the reloading behavior of the MHS specimens in SHPB. The pictures of a deforming MHS specimen between incident and transmitter bars of aluminum SHPB are shown in Fig. 9 at various strain levels. The repeated loading of the MHS specimen is clearly seen in Fig. 9 as the specimen remains between the bars until about relatively large strains. It was also found that the strains measured from the camera recording, simply by measuring the specimen length, and the calculated strains from the SHPB test were very close, varying only about 2–5% from each other. The average strain rate in multiple loading slightly decreased as the number of reloading increased and was found 650 s^{-1} (average) for the first loading and 550 s^{-1} (average) for the sixth reloading. Fig. 10 (a) and (b) show the variation of *R* value with strain in a SHPB multiple loading test and the numerical and experimental stress–strains curves of dynamically and quasi-statically tested samples, respectively. The value of R varies greatly at the beginning of each reloading and the variation decreases as MHS repeatedly reloaded between the bars. Nevertheless, except the first and the second loadings, the variation of *R* values decreases and R values approache zero, showing the attainment of the stress equilibrium between specimen bar interfaces. The model and experimental high strain rate stress values of the tested MHS specimens are also very similar as depicted in Fig. 10(b). The elements chosen for the numerical stress values were

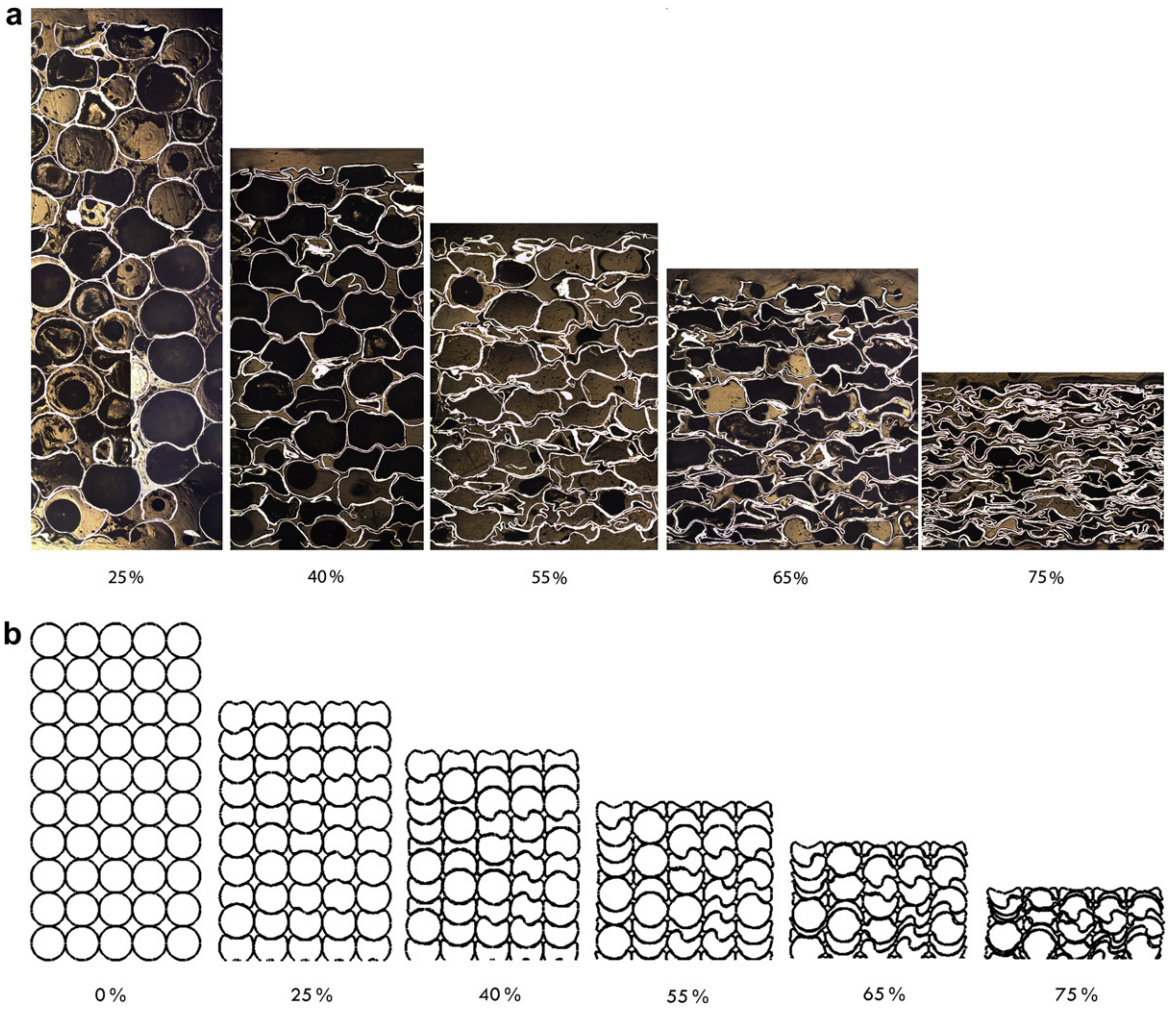

Fig. 6. Dynamically deformed cross-sections of MHS specimens; (a) experimental and (b) model (only one-quarter is shown).

approximately at the same position with the strain gages on the incident and transmitter bars. The MHS structure tested within the studied strain rates further shows a strain rate sensitive collapse stress behavior. The rate sensitivity is also a function of deformation, as the strain increases the rate sensitivity increases as seen in Fig. 10(b).

5. Discussion

The collapse stresses of MHS structures with densities of 300 kg m^{-3} (2 mm spheres) and 600 kg m^{-3} (4 mm spheres) were reported 1.49 and 3.93 MPa, respectively [4]. The measured collapse stress value, 2.12 MPa, for the tested MHS structure with a density of 500 kg m^{-3} is therefore well accord with these values. The effect of strain rate on the collapse behavior of the cellular materials was also previously investigated. Deshpande and Fleck [19] found strain rate insensitive plateau stresses for Alulight closed-cell and Duocell open-cell Al foams up to 5000 s^{-1}. Similar strain rate insensitive plateau stresses were also reported for Alulight closed-cell Al-Si [20] and 6061-Al foams [21]. On the other hand; Mukai et al. [22,23] and Paul and Ramanmurty [18] found an apparent strain sensitive plateau stresses of Alporas Al closed-cell foams. The high strain rate and quasi-static compression testing of MHS structures have shown 55–59% increase in crushing strength when the strain rate increased from quasi-static (4×10^{-4} s^{-1}) to high strain rates (840 s^{-1}) [7]. The strain rate sensitivity was also found to increase with increasing strain in the same study. In an another study, the experimental quasi-static curves of a steel MHS structure was compared with numerical high strain rate compression stress–strain curves (50–1000 s^{-1}) [24]. It was shown an increased strain rate sensitivity with increasing strain and the increased strain rate sensitivity became particularly important after an initial strain of 0.2. The experimentally measured strain rate sensitivity (m) of the tested MHS specimens was calculated between quasi-static (0.8×10^{-4} s^{-1}) and high strain rate (600 s^{-1}) at 0.2 and 0.3 strains using the following relation;

$$m = \frac{\ln \frac{\sigma_H}{\sigma_S}}{\ln \frac{\dot{\varepsilon}_H}{\dot{\varepsilon}_S}} \tag{7}$$

where, H and S stand for the high and quasi-static strain rates, respectively. The strain rate sensitivities of the tested MHS structure were calculated using Eq. (7) and found 0.0167 at 0.2 strain and 0.023 at 0.3 strain. The strain rate sensitivities calculated are however lower than the rate sensitivities calculated for a partial MHS structure (spheres bonded with epoxy), 0.04 [24]. The discrepancy may arise from the epoxy bonding layer used to bond the hollow spheres.

The strain rate sensitive crushing stresses of cellular materials may be attributed to the strain rate sensitivity of the material from which the cellular structure is made, the micro-inertial effects,

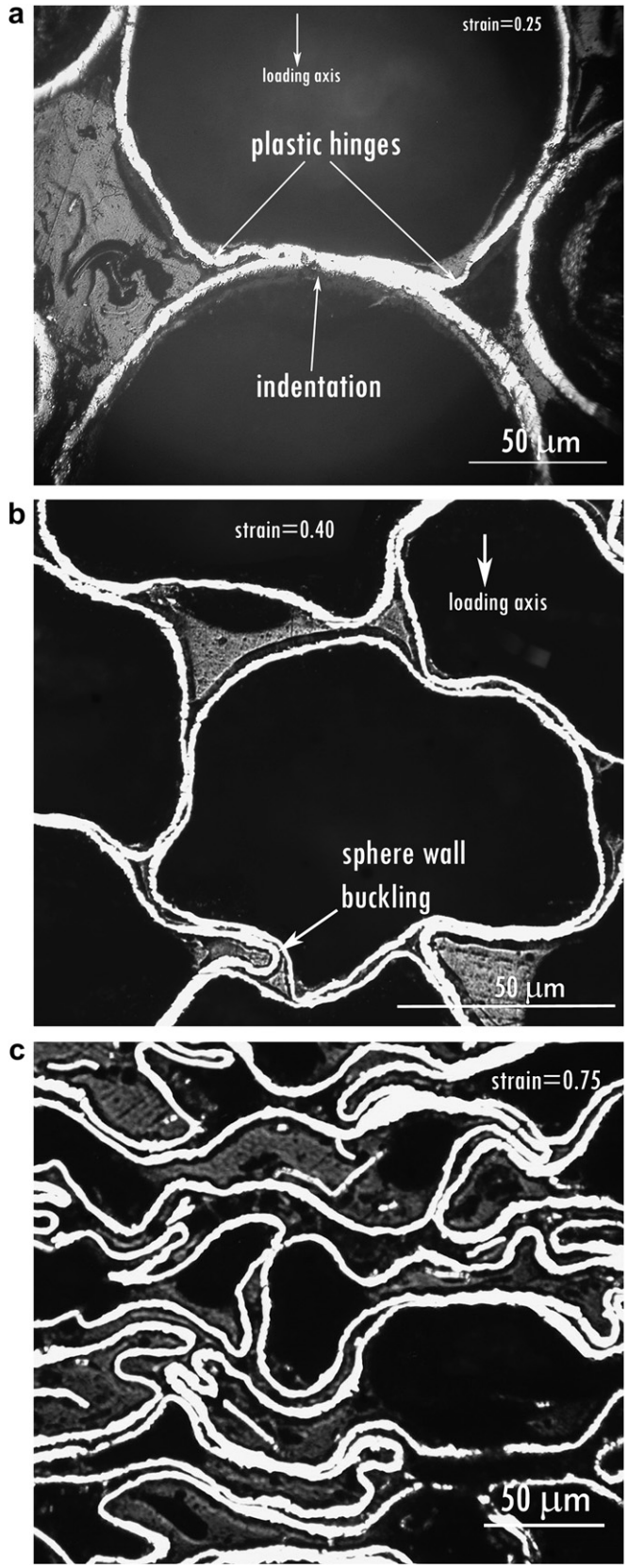

Fig. 7. The deformation mechanism of hollow spheres: (a) plastic hinges and indentation (strain = 0.25), (b) buckling (strain = 0.40) and (c) flattened spheres in the densification region (strain = 0.75).

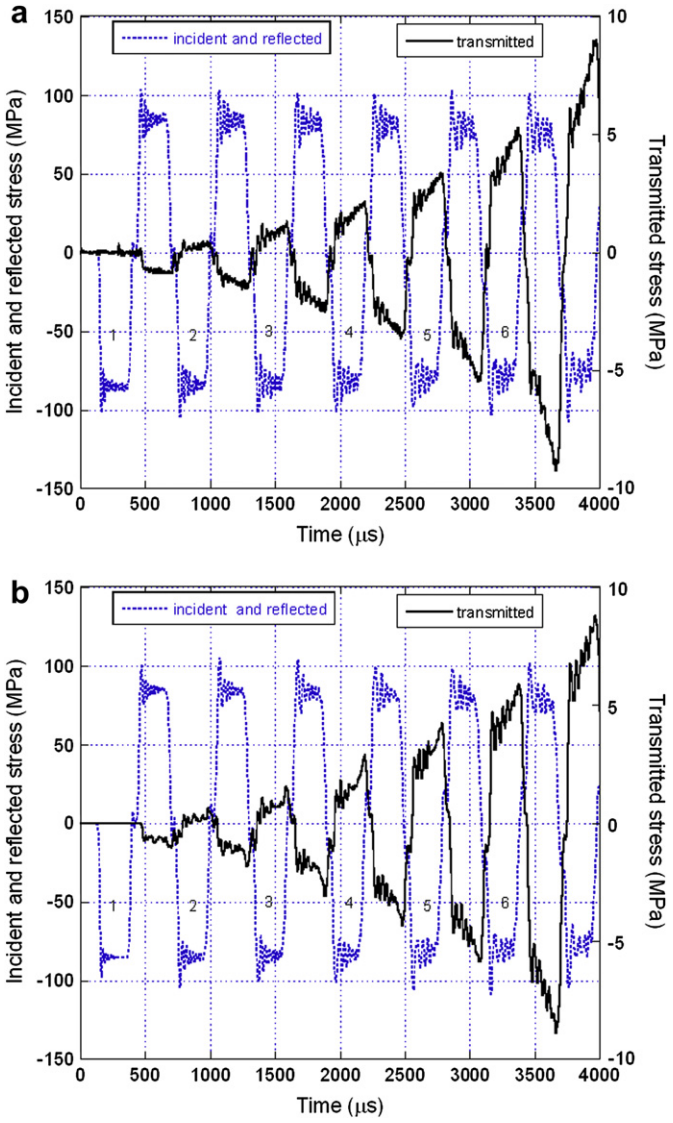

Fig. 8. Variation of incident, reflected and transmitted stresses with time in multiple SHPB loading with a striker bar velocity of 12.5 m s^{-1}: (a) experimental and (b) numerical.

shock wave propagation and the compressed air pressure within the cells [7]. Calculations for adiabatic compression have shown that the compressed air pressure in dynamic loading contributed less than 1.5% of the quasi-static static strength of closed-cell aluminum foams [19]. The calculation used in [19] was repeated for the tested MHS structure with a densification strain of 0.71. Similar contribution of the compressed air was found for the tested MHS structure. At increasing deformation velocities, excess of 50 m s^{-1}, shock wave propagation was shown to have a significant contribution to the strength of the cellular metallic structures [25]. In SHPB testing, the deformation velocities; however, range between 5 and 10 m s^{-1}; therefore, the shock wave propagation enhancement is usually ignored within the strain rate regime of the SHPB testing. Micro-inertial effects arise due to lateral inertia which results in increase of the buckling loads at increasing strain rates [26]. The columnar structures are mainly classified in two groups depending on their response to micro-inertia: Type I and Type II structures [26–28]. Type I structures are characterized with a flat-topped quasi-static stress–strain curves (the stress–strain curve is flat after yielding), showing limited or no strength enhancement at

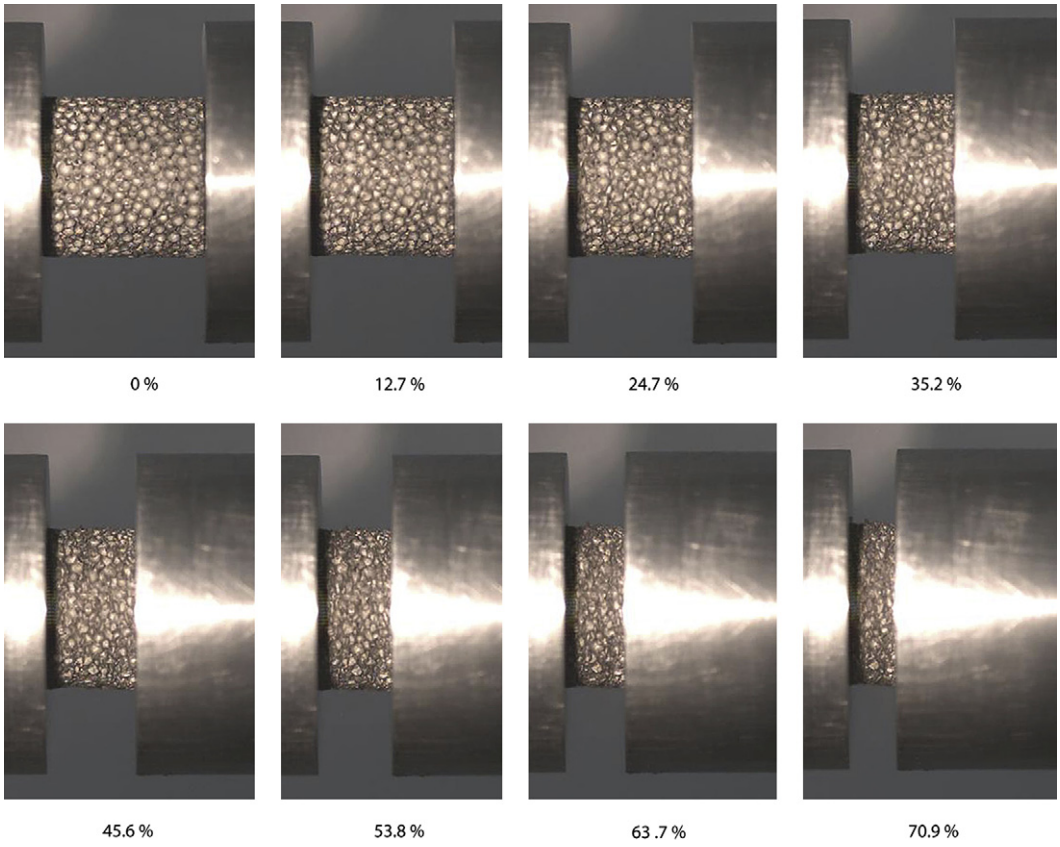

Fig. 9. High speed camera captures of a deforming MHS specimen in SHPB at various strain levels.

increasing deformation velocities. Type II structures are characterized with a strong softening after yielding at quasi-static strain rates and the lateral inertia forces lead to increased bending forces at increasing deformation velocities. The increased deformation forces at increasing strain rates in the compression of aluminum honeycomb structures through out of plane [7], metallic columnar structures [29], aluminum foams [7,18,30,31] and balsa wood in the axial direction [25,32] were reported to result from the micro-inertial effects.

The contribution of strain rate sensitivity of 316 L stainless steel to the strength enhancement of MHS structure tested at increasing strain rates cannot be ignored. The yield strength was shown almost doubled; the stress increased from about 250 MPa at $1\times10^{-3}\,s^{-1}$ to 500 MPa at $2500\,s^{-1}$ [33]. Eq. (6) gives also the similar yield strength values; 260 MPa at $0.8\times10^{-4}\,s^{-1}$ and 531 MPa at $600\,s^{-1}$. The collapse strength of perfect simple cubic packed MHS structure is given as [9],

$$\sigma^{*} = 0.65\sigma_{ys}\left(\frac{\rho^{*}}{\rho_{s}}\right)^{1.36} \tag{8}$$

where, σ^{*} and σ_{ys} are the collapse stress of MHS structure and the yield strength of the cell wall material respectively. Inserting typical values for the studies of MHS structure ($\sigma_{ys}=260$ MPa) into Eq. (8) gives a quasi-static collapse stress of 4.76 MPa, which is at least two times greater than the measured crushing strength. Eq. (8) however assumes a perfect simple cubic packing and excludes the stress degradation resulting from the imperfections such as flat contact regions, porosities on the cell walls, indentation of the spheres and etc. Nevertheless, Eq. (8) predicts a dynamic collapse stress which is two times greater than quasi-static collapse stress, proving a significant contribution of strain rate sensitivity of the cell wall material to the dynamic collapse strength of MHS structure. In order to determine the micro-inertial effects on the high strain rate collapse behavior of the studied MHS structure, the strain rate insensitive material model (quasi-static strength) of 316 L is used to model high strain rate deformation in SHPB. The same experimental striker bar velocity and the geometrical parameters of MHS structure are used in the model. Since the hollow spheres are individually modeled, the micro-inertial effects are automatically taken into account during deformation. The numerical stress–strain behavior of MHS structure at high strain rate with strain rate insensitive cell wall material model is shown in Fig. 11 with that of strain rate sensitive cell material model. The predicted quasi-static stress–strain curve is also shown in Fig. 11. The rate sensitivity of cellular structure was reported to be comparable with that of the cell wall material [34]. The quasi-static curve is therefore predicted by dividing the high strain rate model stress values by the yield strength ratio of dynamic and quasi-static strain rate of cell wall material based on Eq. (8) as,

$$\sigma_{S} = \frac{\sigma_{D}}{\frac{\sigma_{dys}}{\sigma_{sys}}} \tag{9}$$

where, σ_{S}, σ_{D} , σ_{dys} and σ_{sys} are the quasi-static and dynamic crushing strength of the MHS structure and dynamic and quasi-static yield strength of the cell wall material, respectively. The ratio of dynamic and quasi-static yield strength of the studied cell wall material was 2.04 between the studied quasi-static and high strain rate. The difference between the stress values of strain rate insensitive high strain rate deformation and the predicted quasi-static stress values is expected to give the stress value increase arising from the micro-inertial effect as shown in Fig. 11. The contribution of the inertial effects to the stress enhancement at high strain rate is

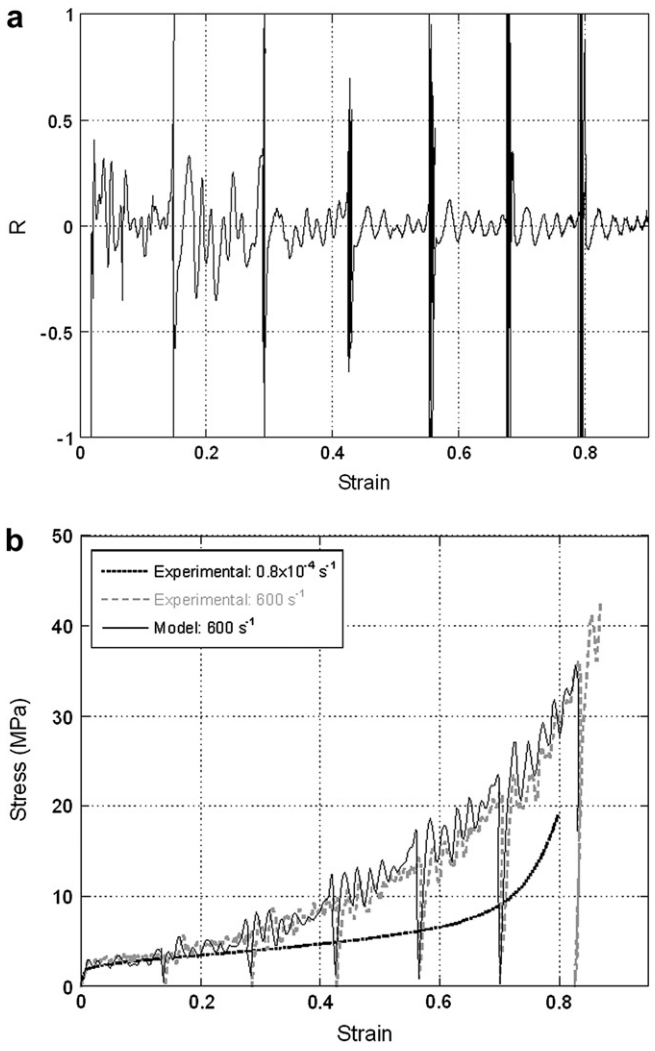

Fig. 10. (a) The variation of R value with strain in SHPB testing and (b) the comparison of numerical and experimental stress–strain curves.

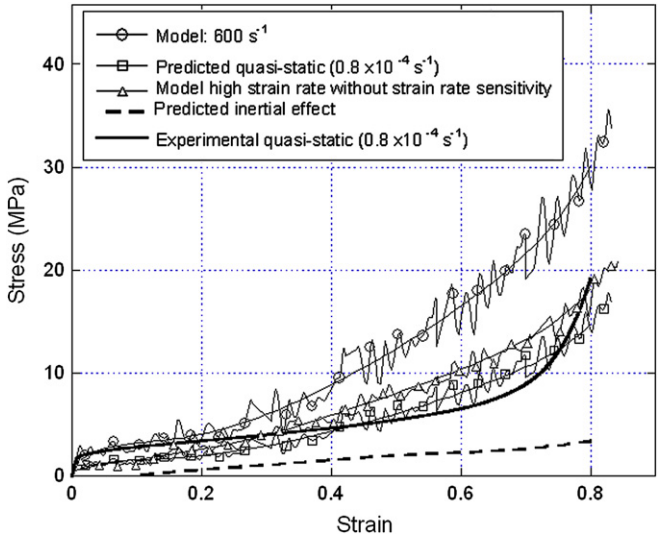

Fig. 11. Quasi-static and the predicted high strain rate stress–strain curves of MHS specimen.

calculated to be 35 and 26% at strain of 0.4 and 0.6, respectively. The increase in the quasi-static stress values due to micro inertia is also predicted 36 and 27% within the studied strain rate limits at 0.4 and 0.6 strain, respectively. The predicted quasi-static stress values in Fig. 11 are however noted to be lower than experimental stress values at strain values lower than 0.4. Above 0.4 strain the predicted stress values are higher than experimental stress values. The differences are partly due to the large variations of R values at lower strains in SHPB testing and a perfectly plastic material model and perfect packing of spheres used for the MHS structure modeling in SHPB testing. The effects of cell wall material model and random packing of spheres on the crushing behavior of MHS structure tested will be analyzed further in a separate study.

The results of modeling efforts of the present study showed that the inertial effects in the testing of MHS structures at increasing strain rates may be significant. It was previously shown that the connection parts which was simulated by a rigid cap, transformed 1D balls from Type I to Type II structure [35]. The connection parts resulted in deformation localization in a single ball, leading the force increase until about a critical value after which the next ball started to deform. This deformation mode is very similar to the deformation behavior of ductile closed-cell aluminum foams in which the deformation in the form of cell wall buckling localizes at a certain region and proceeds to the undeformed sections of the foam sample as the strain increases, resulting in a plateau stress slightly increasing with strain in the collapse region.

6. Conclusions

The high strain rate ($600\ s^{-1}$) compression behavior of a 316 L MHS structure with a density of $500\ kg\,m^{-3}$, an average outer hollow sphere diameter of 2 mm and a wall thickness of 45 μm was investigated both numerically and experimentally. The experimental stress–strain curves at a high strain rate ($600\ s^{-1}$) until about densification strains were obtained through multiple reloading tests using a large diameter compression type aluminum SHPB. For comparison, samples were also compression tested at a quasi-static strain rate ($0.8 \times 10^{-4}\ s^{-1}$). The multiple reloading of MHS sample in SHPB was analyzed with a 3D finite element model using the commercial explicit finite element code LS-DYNA. Two materials models were used in the model; the strain rate sensitive and the strain rate insensitive cell wall material model. Results have shown that crushing strength of the tested MHS samples increase with increasing strain rate and strain. Quasi-statically and dynamically deformed MHS samples showed similar deformation characteristics, plastic hinge formation and the indentation of the spheres at the contact regions at relatively low strains and the sphere wall buckling at increasing strains. Assuming the rate sensitivity of MHS structure was similar to that of the cell wall material and modeling MHS structure SHPB testing with a rate insensitive cell wall material, the extend of micro-inertial effects was predicted. Based on the predictions, the strain rate sensitivity of the studied 316 L MHS structure was attributed to the strain rate sensitivity of the cell wall material and the micro-inertial effects. Within the studied strain rate limits, the contribution of the cell wall material rate sensitivity to the increased stress values at high strain rate was found to be higher than that of inertial effects for 316 L MHS structure investigated.

Acknowledgement

The authors would like to thank the Scientific and Technical Council of Turkey (TUBITAK) for the grant # 106M353. The authors are grateful to the Fraunhofer Institute IFAM for supplying MHS materials.

References

[1] Gibson LJ. Mechanical behavior of metallic foams. Annu Rev Mater Sci 2000;30:191–227.
[2] Ramamurty U, Paul A. Variability in mechanical properties of a metal foam. Acta Metall Mater 2004;52:869–76.
[3] Andersen O, Waag U, Schneider L, Stephani G, Kieback B. Novel metallic hollow sphere structures. Adv Eng Mater 2000;2:192–5.
[4] Friedl O, Motz C, Peterlik H, Puchegger S, Reger N, Pippan R. Experimental investigation of mechanical properties of metallic hollow sphere structures. Metall Mater Trans B 2008;39:135–46.
[5] Lim TJ, Smith B, McDowell DL. Behavior of a random hollow sphere metal foam. Acta Metall Mater 2002;50:2867–79.
[6] Vesenjak M, Fiedler T, Ren Z, Ochsner A. Behaviour of syntactic and partial hollow sphere structures under dynamic loading. Adv Eng Mater 2008;10:185–91.
[7] Zhao H, Elnasri I, Abdennadher S. An experimental study on the behaviour under impact loading of metallic cellular materials. Int J Mech Sci 2005;47:757–74.
[8] Karagiozova D, Yu TX, Gao ZY. Modelling of mhs cellular solid in large strains. Int J Mech Sci 2006;48:1273–86.
[9] Sanders WS, Gibson LJ. Mechanics of bcc and fcc hollow-sphere foams. Mat Sci Eng A-Struct 2003;352:150–61.
[10] Sanders WS, Gibson LJ. Mechanics of hollow sphere foams. Mat Sci Eng A-Struct 2003;347:70–85.
[11] Guden M, Hall IW. High strain-rate compression testing of a short-fiber reinforced aluminum composite. Mat Sci Eng A-Struct 1997;232:1–10.
[12] LSTC. LS-DYNA keyword user's manual. Livermore Software Technology Corporation; 2007.
[13] Ravichandran G, Subhash G. Critical-appraisal of limiting strain rates for compression testing of ceramics in a split hopkinson pressure bar. J Am Ceram Soc 1994;77:263–7.
[14] Tasdemirci A, Hall IW, Gama BA, Guden M. Stress wave propagation effects in two- and three-layered composite materials. J Compos Mater 2004;38:995–1009.
[15] Schleyer GK, Lowak MJ, Polcyn MA, Langdon GS. Experimental investigation of blast wall panels under shock pressure loading. Int J Impact Eng 2007;34:1095–118.
[16] Fallet A, Lhuissier P, Salvo L, Brechet Y. Mechanical behaviour of metallic hollow spheres foam. Adv Eng Mater 2008;10:858–62.
[17] Chan KC, Xie LS. Dependency of densification properties on cell topology of metal foams. Scripta Metall Mater 2003;48:1147–52.
[18] Paul A, Ramamurty U. Strain rate sensitivity of a closed-cell aluminum foam. Mat Sci Eng A-Struct 2000;281:1–7.
[19] Deshpande VS, Fleck NA. High strain rate compressive behaviour of aluminium alloy foams. Int J Impact Eng 2000;24:277–98.
[20] Peroni L, Avalle M, Peroni M. The mechanical behaviour of aluminium foam structures in different loading conditions. Int J Impact Eng 2008;35:644–58.
[21] Hall IW, Guden M, Yu CJ. Crushing of aluminum closed cell foams: density and strain rate effects. Scripta Metall Mater 2000;43:515–21.
[22] Mukai T, Kanahashi H, Miyoshi T, Mabuchi M, Nieh TG, Higashi K. Experimental study of energy absorption in a close-celled aluminum foam under dynamic loading. Scripta Metall Mater 1999;40:921–7.
[23] Mukai T, Miyoshi T, Nakano S, Somekawa H, Higashi K. Compressive response of a closed-cell aluminum foam at high strain rate. Scripta Metall Mater 2006;54:533–7.
[24] Vesenjak M, Ren Z, Ochsner A. Behaviour of cellular materials under impact loading. Material Wiss Werkst 2008;39:125–32.
[25] Reid SR, Peng C. Dynamic uniaxial crushing of wood. Int J Impact Eng 1997;19:531–70.
[26] Calladine CR, English RW. Strain-rate and inertia effects in the collapse of 2 types of energy-absorbing structure. Int J Mech Sci 1984;26:689–701.
[27] Su XY, Yu TX, Reid SR. Inertia-sensitive impact energy-absorbing structures .1. Effects of inertia and elasticity. Int J Impact Eng 1995;16:651–72.
[28] Su XY, Yu TX, Reid SR. Inertia-sensitive impact energy-absorbing structures .2. Effect of strain-rate. Int J Impact Eng 1995;16:673–89.
[29] Langseth M, Hopperstad OS. Static and dynamic axial crushing of square thin-walled aluminium extrusions. Int J Impact Eng 1996;18:949–68.
[30] Zhao H, Elnasri I, Li HJ. The mechanism of strength enhancement under impact loading of cellular materials. Adv Eng Mater 2006;8:877–83.
[31] Lee S, Barthelat F, Moldovan N, Espinosa HD, Wadley HNG. Deformation rate effects on failure modes of open-cell al foams and textile cellular materials. Int J Solids Struct 2006;43:53–73.
[32] Tagarielli VL, Deshpande VS, Fleck NA. The high strain rate response of pvc foams and end-grain balsa wood. Compos Part B-Eng 2008;39:83–91.
[33] Xue Q, Gray GT. Development of adiabatic shear bands in annealed 316l stainless steel: Part i. Correlation between evolving microstructure and mechanical behavior. Metall Mater Trans A 2006;37A:2435–46.
[34] Han FS, Cheng HF, Li ZB, Wang Q. The strain rate effect of an open cell aluminum foam. Metall Mater Trans A 2005;36A:645–50.
[35] Ruan HH, Gao ZY, Yu TX. Crushing of thin-walled spheres and sphere arrays. Int J Mech Sci 2006;48:117–33.